RSC Advances

ROYAL SOCIETY OF CHEMISTRY

www.rsc.org/advances

RSC Advances

ARTICLE

pH-Sensitive nanomedicine based on PEGylated nanodiamond for enhanced tumor therapy

Lin Li,[a] Lu Tian,[b] Wenjing Zhao,[b] Fangqin Cheng,[c] Yingqi Li*[a,b] and Binsheng Yang*[a]

Received 00th January 20xx,
Accepted 00th January 20xx

DOI: 10.1039/x0xx00000x

www.rsc.org/

Enhancing chemotherapeutic efficiency through enriched drug load and controlled drug release is urgent for alleviate the suffering of cancerous patients. Here, a novel pH-sensitive nanomedicine was constructed to acquire high drug capacity and better therapeutic efficiency. Interestingly, with the assistance of pH 8.0 sodium borate buffer solution, PEGylated Nanodiamond vehicles loaded with doxorubicin (DOX) achieved nearly 50% loading efficiency, low premature drug release in physiological conditions and effectively stimuli-responsive release under the tumor microenvironment. Besides, assessments of flow cytometer and cell migration illustrated NP/D could induce cell apoptosis, cycle abnormality and inhibit cell migration. The results from the confocal fluorescence microscopy study showed that NP/D could be internalized into cells and distributed into cytoplasm, subsequently DOX detached from NP/D could migrate and enter the nucleus to inhibit cell proliferation. The NP/D can be open the new nanodrugs window for a broad spectrum of anticancer agents.

1. Introduction

In order to overcome the severe side effects induced by chemotherapy agents during cancer therapy,[1,2] a wide range of nanocarriers, such as, iron oxide magnetic nanoparticles,[3] gold nanoparticles[4] and polymer nanoparticles[5] were explored to delivery anticancer drug so as to enhance efficiency of chemotherapy. However, despite many advantages of nanocarriers promote their availability, the instability and toxicity of the nanocarriers limited their further clinical application.[6-9]

Nanodiamond (ND), a new family member of carbon nanoparticles, has been unearthed for various biomedical applications.[10-13] ND has been a nouveau nanocarrier for drug delivery[14-16] and cellular imaging,[17] which is due to not only possess least toxicity compared to other carbon-based materials, excellent biocompatibility, chemical stability and optical properties,[18-20] but also could be modified to make it have more virtues.[21-23] Choi etal. demonstrated that ND could improve the cellular uptake of DOX and be employed as drug carriers for efficient cancer therapy.[24] Ho etal. also demonstrated DOX complexed with ND and administered via convection-enhanced delivery (CED) was significantly more efficient at killing tumor cells than uncomplexed DOX and suggest that CED of ND-DOX is a promising approach for brain tumor treatment.[25] Our previous study also established FND-DOX system and found slow and sustained drug release capability.[26] Despite researches showed ND could improve antitumor activity of free DOX, the widely application in biology of ND has been limited due to the trend to aggregate.[27]

Nanoparticles functionalized with polymer and protein has been demonstrated enhanced circulation time and increased dispersibility.[28-30] poly (ethylene glycol) (PEG) has been introduced onto ND, which can not only improve the dispersion, but also reduce the interaction with cells to reducing non-specific effects, and prolong the blood circulation time.[31,32] Our previous study verified transferrin and PEG improved the dispersibity of ND and prolonged the cellular uptake half-life,[33-36] whereas the loading efficiency and treatment efficiency are still not so satisfactory.

Taking into account the enhancement drug loading and treatment efficiency for tumor, a novel nanodrug based on free DOX physical adsorption onto PEGylated ND in the pH 8.0 sodium borate buffer solution was designed. Specifically, carboxylated ND was conjugated by polyethylene glycol amine carboxyl (H_2N-PEG-COOH) to obtain the ND-PEG nanocarrier. In the following step, DOX was successfully coated onto the ND-PEG in the pH 8.0 sodium borate buffer solution via electrostatic interactions to obtain ND-PEG/DOX (NP/D) nanoparticles. We found that the addition of pH 8.0 sodium borate buffer solution is an essential component of the loading process and it was shown to be able to promote the adsorption of DOX onto the PEGylated NDs, where nearly 50%wt adsorption of DOX on the ND-PEG was achieved in the pH 8.0 sodium borate buffer solution. The NP/D was found to move inside the cells quickly and was capable of ferrying the drug inside living cells efficiently. In addition, NP/D showed a higher cytotoxicity with time increase than that of the free DOX. As such, this work convincingly demonstrates the potential of ND as a broad drug-functionalization platform.

2. Experimental section

2.1. Materials and instruments

[a] Key Laboratory of Chemical Biology and Molecular Engineering of Ministry of Education, Institute of Molecular Science, Shanxi University, Taiyuan 030006, PR China. *E-mail: wkyqli@sxu.edu.cn, yangbs@sxu.edu.cn
[b] Department of Chemistry, College of Chemistry and Chemical Engineering, Shanxi University, Taiyuan 030006, PR China.
[c] Institute of Environmental Science, Shanxi University, Taiyuan 030006, PR China.
Electronic Supplementary Information (ESI) available: [cell viability with time, cell morphology and cellular uptake kinetics]. See DOI: 10.1039/x0xx00000x

Synthetic type 1b nanodiamond powders (ND) which is commercially available (sizes ≈140 nm, Element Six) were chosen in the experiment because the tumor blood vessels can retain 100-400 nm particles. Carboxylated ND that used in the experimental part was obtained according to previously reported method by us. Doxorubicin hydrochloride (DOX) was purchased from Shanxi pude Pharmaceutical Co., Ltd. (China). Polyethylene glycol amine carboxyl (H_2N-PEG-COOH, Mw: 2000) was bought from Shanghai seebio Biotech Inc, China. Fluorescamine was bought from TCI (Shanghai) Chemical Industry (China). N-hydroxy succinimide (NHS), 2- (N-morphine) ethane sulfonic acid (MES) and 1- (3-dimethylaminopropyl)-3-ethyl carbodiimide hydrochloride (EDC) were purchased from Sigma. (M-β-CD) were purchased from Shanghai Aladdin Reagent Co., Ltd. (China). 3-(4, 5-dimethylthiazol-2-yl)-2, 5-diphenyltetrazolium bromide (MTT), Penicillin-streptomycin combination and paraformaldehyde were purchased from Solarbio (Beijing, China). Dulbecco Minimum Essential Media (DMEM) was purchased from Thermo Fisher Biological and Chemical Product (Beijing, China). Fetal bovine serum was purchased from Hangzhou Sijiqing Biological Engineering Materials Co., Ltd (China). Trypsin was purchased from Sino-American Biotechnology Company. Hoechst 33258 was purchased from Beyotime Biotechnology (in China). Sucrose was purchased from Amresco Co. (USA). HeLa, HepG2 and MCF-7 cells were provided by the Gene Engineering Center of Shanxi University. All other chemicals and solvents were of analytical grade and procured from local suppliers unless otherwise mentioned. Millipore filtered water was used for all aqueous solutions.

Fluorescence spectrophotometer (970CRT, Shanghai Analytical Instruments Factory), UV-visible spectrophotometer (UV1901, Beijing spectral analysis of GM), Ultrasonic cleaner (KQ-100DE, Kunshan Ultrasonic Instrument Co., L,), High speed micro-centrifuges (TG16-W, Hunan Instrument Laboratory Instrument Development Co., Ltd.), Flip shake instrument (DR-MIX, Beijing Hao North Biotechnology Co., Ltd.), Air oscillator (THZ-22, Taicang City Experimental Equipment Factory), Fourier transform infrared spectroscopy (FTIR-8400S, Shimadzu Corporation, Kyoto, Japan), Malvern Nano Particle Sizer (ZETA Sizer, Nano-ZS90, England), Autoclave (YX280B, Shanghai Medical Devices Co., Ltd.), Transmission electron microscopy (JEM-2100, JEOL, Japan), Vacuum drying oven (DZF-6020, Shanghai Yiheng Scientific Instrument Co., Ltd.), Thermostat water bath (ZDKW-4, Beijing Zhongxing Weiye Instrument Co., Ltd.), Inverted microscope (MI11, Guangzhou Mingmei Technology Co., Ltd.), Optical microscope (XSP-8CA, Shanghai Optical Instrument Factory), Clean bench (YT-CG-1ND, Beijing Both Cologne Experiment Technology Co., Ltd.), Full automatic microplate reader (Model 550, Bio-Rad, USA), Flow cytometer (FACS Calibur, BD, USA), Laser scanning confocal microscope (Leica TCSSP5, Germany).

2.2. Optimization and Preparation of ND-PEG/DOX

2.2.1. The pH effect on DOX adsorption. First, ND-PEG was prepared following previously reported procedure.[36] Then six 1 mg of ND-PEG nanoparticles were sonicated at 100 W for 30 minutes in 1 mL of different buffer solution (4.0, 6.0, 7.0, 8.0, 9.0 and 10.0). Next, 100 μg of doxorubicin was added, and the suspension was shaken and protected from light at room temperature for 6 h. Finally, the suspension was centrifuged at 15000 rpm for 5 minutes, and the precipitate was washed three times with corresponding buffer solution to remove the unadsorbed DOX. The amount of DOX adsorbed was determined by calculating the change in DOX concentration before and after adsorption using an ultraviolet-visible spectrophotometer at 495 nm.

2.2.2. The time effect on DOX adsorption. Based on the optimum pH effect between ND-PEG and DOX, the optimum reaction time between ND-PEG and DOX was also investigated in pH 8.0 sodium borate buffer solution using the technique as previously reported by us.[36]

2.2.3. Drug loading efficiency. Based on the optimum pH effect and reaction time between ND-PEG and DOX, the amount of drug loading was further researched, where the concentrations of DOX were 100, 200, 500, 600, 1000 μg·mL^{-1} and the concentration of ND-PEG was 1mg·mL^{-1} for all solutions in pH 8.0 sodium borate buffer solution for 6 h. Then the solutions were centrifuged at 15000 rpm for 5 min to remove excessive DOX. As previous reported,[37] briefly, the supernatants were removed, and their absorbance was read from 200 to 800 nm at ambient temperature with a UV-visible spectroscopy. The peak absorbance of DOX was found at 495nm. The difference in added DOX and DOX in the supernatant yielded the amount of DOX adsorbed. The drug loading efficiency and drug loading percentage on ND-PEG were assessed using the following equations (1) and (2), respectively:

$$\frac{\mathrm{DOX\ (\mu g)_{Adsorbed}}}{\mathrm{DOX(\mu g)_{Added}}} \times 100\% \quad (1) \qquad \frac{\mathrm{DOX\ (\mu g)_{Adsorbed}}}{\mathrm{ND-PEG(\mu g)_{Added}}} \times 100\% \quad (2)$$

2.2.4. Preparation of ND-PEG/DOX. In the subsequent experiments, the as-prepared NP/D nanoparticles with DOX loading of 99.5 μg/mg were characterized and studied. ND-PEG (1 mg) was dispersed in the pH 8.0 sodium borate buffer and sonicated for 30 min, DOX (200 μg) was then added and the mixture was shaken up at room temperature for 6 h. ND-PEG/DOX (NP/D) thus obtained by centrifugation at 15000 rpm, rinsed with pH 8.0 sodium borate buffer for three times and then placed in a vacuum drying oven and protected from light. The amount of absorbed DOX was measured by calculating the difference value of the total DOX and the supernatant DOX.

2.3. Characterization of ND-PEG/DOX

Fourier transform infrared spectroscopy (FTIR) and UV-visible spectroscopy were used to confirm the presence of the DOX and PEG on the surface of ND. A Zeta-sizer Nano ZS90 was used to monitor the zeta potential, polydispersity index (PDI) and hydrodynamic size of the ND before and after modification. Measurements of nanoparticles size were performed at 25 °C and a scattering angle of 90°. The mean hydrodynamic diameter was determined by cumulative analysis. Determination of the zeta potential was based on electrophoretic mobility of the nanoparticles in aqueous medium, and was performed using folded capillary cells in automatic mode. The dispersion of ND, ND-PEG and ND-PEG/DOX in distilled water was observed by a digital camera.

2.4. In vitro drug release

The DOX release study was carried out in dialysis bags at 37 °C in phosphate buffer solutions (pH 7.4, 6.5 and 5.0) with air oscillator. Firstly, 1 mL ND-PEG/DOX suspension that well dispersed was placed in a dialysis tube. Then the dialysis bag was quickly immersed in 9mL of the corresponding PBS solutions in an air oscillator keeping the shaking (150 rpm) and a changeless temperature (37 °C). At the scheduled time, 2 mL sample was withdrawn and the same amount of fresh release medium was replenished. The amount of released DOX was measured with the ultraviolet measurements at the wavelength of 480 nm.

2.5. Cell culture

HepG2, HeLa and MCF-7 cells were obtained from the Gene Engineering Center of Shanxi University. All cells were cultured in plastic dishes containing DMEM supplemented with 10% FBS and 1% penicillin-streptomycin in a CO_2 incubator at 37 °C and passaged every 2 days using trypsin containing EDTA and PBS (pH 7.4).

2.6. In vitro viability

The in vitro viability assay was performed as described previously.[36] Briefly, 5000 cells/well in the case of HepG2, HeLa and MCF-7 cells were seeded into the 96-well plates with 200 μL per well and treated with ND-PEG, NP/D or free DOX at a series of various concentrations for 72 h. After 72h, a stocked MTT solution (5 μg·mL^{-1}) was added and incubated for another 4 h. Thereafter, the medium was discarded, and 150 μL of dimethyl sulfoxide was added. After 10 min of vibration, absorbance at 490 nm was read by a microplate reader.

2.7. In vitro wound scratch assay

The scratch assay was performed as the previous reported.[38] Firstly, the MCF-7 cells were plated onto each well of the six-well plate at a density of 2×10^5 to create a confluent monolayer, and then incubate the cells properly for approximately 20 h at 37 °C, allowing the cells to adhere and spread on the substrate completely. After that, the cell monolayer were scraped in a straight line to create a wound scratch with a sterile pipette of 10 μL, the injured cells were removed by washing thrice with PBS (pH 7.4), followed adding control fresh medium or medium with ND-PEG, NP/D and free DOX and continue to develop for a period of time. Finally, place the six-well plate under a phase-contrast microscope and take images of each sample at the predetermined time. The images can be analyzed quantitatively by using computing software of choice. The wound closure rate and migration inhibiting rate was calculated by the following equation:

$$\mathrm{WC} = \left(1 - \frac{\mathrm{sw_t}}{\mathrm{sw_0}}\right) \times 100\%, \quad \mathrm{MIR} = \left(1 - \frac{\mathrm{wc_{treatment}}}{\mathrm{wc_{control}}}\right) \times 100\%$$

where SW_0 and SW_t stand for the scratch width of 0h and given time, respectively, $WC_{treatment}$ and $WC_{control}$ stand for the wound closure rate of treatment and control groups.

2.8. Cellular uptake

MCF-7 cells were sowed into the confocal laser special dish at a density of 1×10^3 per dish overnight at 37 °C under a 5% CO_2 atmosphere. Then the culture medium was withdrawn and replaced with fresh medium containing 5 μg·mL^{-1} NP/D. After incubation for 2h and 5h, respectively, the cells were fixed with 4% paraformaldehyde and then stained with Hoechst 33258. At last, the cells were observed by confocal laser scanning microscopy (CLSM). Samples stained with H33258 and DOX were visualized with excitation wavelengths of 405 nm and 488 nm, respectively.

2.9. Cell apoptosis and cell cycle assay

MCF-7 cells in fresh complete medium were cultured (1×10^5) into 35 mm petri dishes for 16h. After complete adhesion, the cells were treated with NP/D (5 μg·mL^{-1}) for another 48h. The cells were then collected with trypsin, washed twice with cold PBS (pH 7.4). After that, the cells were resuspended in PBS and stained by both Annexin V-FITC (5 μL) and PI (5 μL) in dark condition for 15-20 min. Finally, the cells were analyzed by an FACS Calibur flow cytometer.

MCF-7 cells were cultured in 60 mm culture dish at a density of 1×10^6 and incubated for 16-20 h to make the cells adhere completely. After incubation, the cells were washed with PBS (pH 7.4) three times and cultured with NP/D or free DOX at a concentration of 5 μg·mL^{-1} for another period of time. When the treatment was over, the cells were collected, washed twice with cold PBS (pH 7.4) and fixed with ice-cold 70% ethanol overnight at 4 °C. Sample cells prepared for the flow cytometry analysis were treated with RNase and propidium iodide (PI) for 30 min at room temperature in the dark.

3. Results and discussion

3.1. Synthesis and Characterization of ND-PEG/DOX

To increase the antitumor activity of DOX, simultaneously decrease the side effects of DOX in the normal tissue and improve the dispersity of nanodiamond, a relatively stable amide bond was introduced to conjugate H_2N-PEG-COOH and ND, to produce ND-PEG by one step activation of carboxyl groups and the other step esterification of amine groups as previously reported.[36,39] The synthesis route is presented in Scheme 1. Meanwhile, a promising drug delivery system based on PEGylated nanodiamond bearing the anticancer drug DOX was also obtained in the presence of sodium borate buffer solution which pH is 8.0. In the work, we achieved high DOX loading content near 49.9 wt % adsorption of DOX on the PEGylated nanodiamond. The loading mechanism of adsorption of DOX onto the PEGylated nanodiamond can be explained as follows: Because doxorubicin is a weak base with a pK_b of 8.3, doxorubicin in buffer solution with a pH of 8.0 would result in ionized NH^{3+} and would balance with the carboxyl groups on ND-PEG via electrostatic interaction. Besides, due to the grafting amount of PEG onto nanodiamond is 150 μg/mg (Fig. S1), the amount of carboxyl on the ND is redundant (the total amount of carboxyl on the ND is 1.26× 10-7 μmol/mg[40]), so DOX also can be adsorbed onto the carboxylic groups of nanodiamond. Moreover, the ND-PEG/DOX (NP/D) complexes may be the result of vander Waals forces between doxorubicin molecules and carboxylic groups on the ND-PEG or ND as previously described.[41]

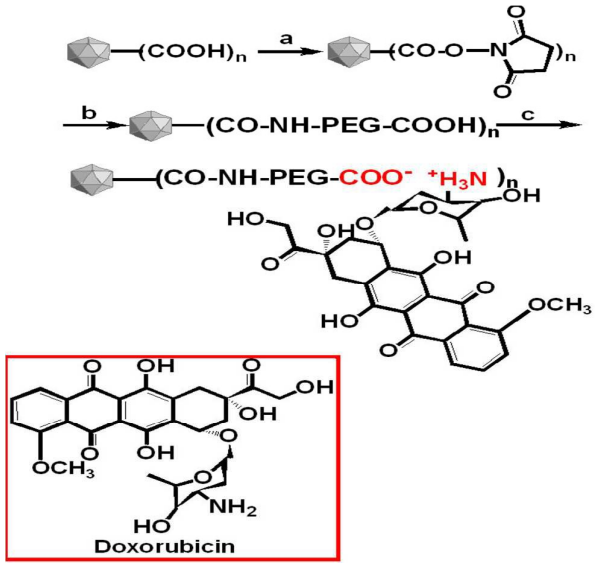

Scheme 1 Synthesis of ND-PEG/DOX. The succession of synthetic processes is the following: (a) EDC, NHS, MES (0.1M, pH 5.8), rt, 6h; (b) H_2N-PEG-COOH, BBS (pH 8.4), rt, overnight; (c) DOX, BBS (pH 8.0), rt, 6h.

Table 1 Summary of added DOX, absorbed DOX, DOX loading efficiency and DOX loaded on ND-PEG.

DOX Added μg	DOX Adsorbed μg	DOX Loading efficiency (%)	DOX Loaded on ND-PEG (%)
100	46.9±1.2	46.2±0.7	4.7±0.2
200	99.5±0.9	49.8±0.9	10.0±0.3
500	249.2±1.3	49.8±0.6	24.9±0.3
600	301.6±1.1	50.3±0.4	30.2±0.4
1000	498.5±1.0	49.9±1.0	49.9±0.6

To improve the amount of drug loaded onto the ND-PEG nanoparticles, first, the adsorption of DOX with different pH values was explored as shown in Fig. 1A. We can observe that the maximum amount of DOX adsorption was pH 8.0. Subsequently, the amount of DOX loaded as a function versus time was displayed in Fig. 1B. One can observe that a dynamic equilibrium process of adsorption and dissociation exists between DOX and ND-PEG as our previously reported.[36] Specifically, (1) within 2.5 h, the dissociation rate accounts for the main control position, resulting in the amount of DOX adsorbed on the nanoparticles decreasing with time; (2) within 3 – 6 hours, the adsorption rate is greater than the dissociation rate, resulting in the amount of DOX adsorbed on nanoparticles increasing with time; however, after six hours, a dynamic equilibrium process between dissociation and adsorption occurred, and thus the amount of drug adsorbed on the nanoparticles no longer changed. This behavior follows the first-order kinetics. In the system, the amount of DOX adsorbed was determined through converting the UV-Vis absorbance to concentration using linear regression equation (Fig. S2).

Table 1 summarizes the adsorbed DOX, DOX loading efficiency, and DOX loading on ND-PEG. NDs adsorbed 99.5 μg of the added 200 μg DOX, which yielded a 49.8 % loading efficiency. When 1000 μg DOX was added, the ND-PEG adsorbed approximately 498.5 μg DOX corresponding to a DOX loading efficiency of about 49.9 %. Since 1.0 mg of ND-PEG was used, loadings of DOX on the ND-PEG can up to 49.9 % for the added 1000 μg DOX. The DOX loading on ND-PEG and drug loading efficiency achieved with our adsorption technique were much higher than that of our reported for ND-PEG/DOX complexes,[35] Which was almost sixteen fold increase in DOX loading onto the ND-PEG in the best conditions.

To confirm synthesis, the surface chemistry, particle size, polydispersity index (PDI) and zeta potential of the NP/D were characterized. Fig. 2A shows the FTIR of ND, ND-PEG, NP/D, H_2N-PEG-COOH and DOX. Compared to the spectrum of ND, The peak at 1656 cm^{-1} and 1621cm^{-1} correspond to the C=O stretching and N-H bending, respectively, which are represent the characteristic peaks of amide linkage, confirming that H_2N-PEG-COOH was coupled onto ND successfully. In the spectrum of NP/D, the peaks at 1402 cm^{-1}, 1087 cm^{-1} and 803 cm^{-1} are attributed to the characteristic peaks of DOX as black arrow indicated, therefore, the FTIR results supported that DOX was also absorbed onto ND-PEG.

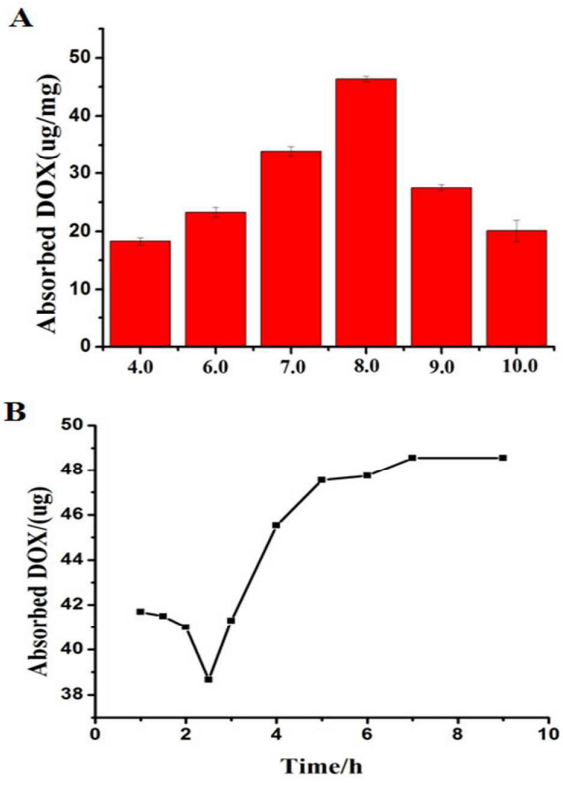

Fig. 1 Optimal conditions for preparing the NP/D system. (A) Determination of the best pH for adsorption of DOX. (B) Determination of the best time for adsorption of DOX.

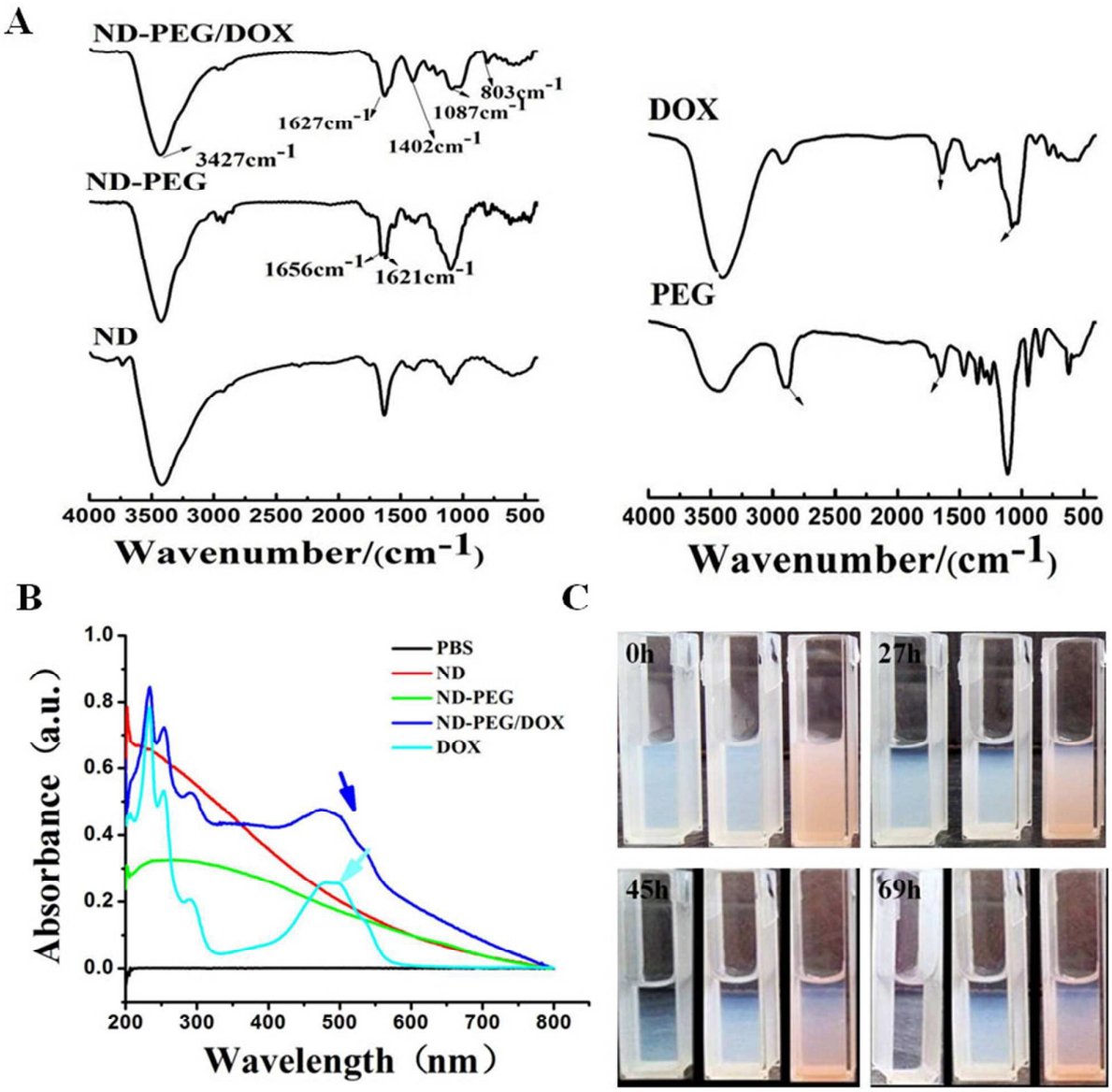

Fig. 2 Characterization of ND-PEG/DOX. (A) FTIR Spectra of various materials. (B) UV-Vis absorption of DOX, ND, ND-PEG and ND-PEG/DOX in PBS (pH 7.4). (C) The dispersity of different nanoparticles in PBS 7.4 with time (the left is ND, the middle is ND-PEG, the right is NP/D).

Fig. 2B depicts the absorption spectra measured by UV-Vis spectrometer for ND, ND-PEG, NP/D, and free DOX. The ND and ND-PEG has no absorption peak, while NP/D revealed a pronounced absorption with a peak at 480 nm just as the free DOX, which suggested the successful loading of DOX onto the surface of ND-PEG.

To further estimate the potential of using NP/D as an anti-tumor therapeutic agent, the dispersity of NP/D was also investigated. Due to the easy aggregation of ND, H_2N-PEG-COOH was introduced to functionalize the ND through covalent interaction of amido bond, forming PEGylated ND with good dispersibility. The test results were showed in Fig. 2C. As the photos shown, after stewing 69 h, ND was almost to settlement entirely, while ND-PEG and NP/D still kept a good dispersibility, which verify that H_2N-PEG-COOH can offer the NP/D with favorable dispersity, better to prove that NP/D can be as the antitumor agent.

The ND-PEG and NP/D were further analyzed by the DLS and Zeta potential technique, and the data was given in Table 2. As shown in Table 2, DLS results showed that the average size of unmodified ND is 166.0 ± 1.6 nm, after coupling with H_2N-PEG-COOH, the size

Table 2 PDI、Particle size and Zeta potential of ND, ND-PEG and ND-PEG/DOX

	Diameter（nm）	Zeta potentials（mV）	PDI
ND	166.0±1.6	-30.2±1.0	0.164
ND-PEG	184.6±6.4	-24.7±1.9	0.126
NP/D	195.0±1.3	-20.8±0.4	0.089

increased to 184.6 ± 6.4 nm, which was further confirmed that H_2N-PEG-COOH was connected to ND as FTIR spectrum verified. And that the size of NP/D is about 195.0 ± 1.3 nm with a PDI of 0.089, which indicated that very suitable for drug delivery. In addition, the zeta potential of the above mentioned nanoparticles was measured (Table 2), ND has a relatively negative initial zeta potential of -30.2 ± 1.0 mV, along with the successfully synthesized of ND-PEG (-24.7 ± 1.9 mV) and ND-PEG/DOX (-20.8 ± 0.4 mV), the zeta potential is slowly increasing, which indicated that PEG and DOX successfully coated onto the surface of ND.

3.2. In vitro drug release

The ND-PEG/DOX drug delivery system is designed for tumor micro-environment release of DOX. Since the pH of blood and normal tissues is around 7.4, and the pH values of tumor micro-environment are much lower (at pH 5.0-6.5),[42] the pH-sensitive releasing property of the NP/D nanocomposite will facilitate drug delivery. To verify the pH-sensitive release of DOX in vitro, NP/D samples were incubated at a simulated physiological condition (pH 7.4) and in an acidic tumor micro-environment (pH 5.0 and 6.5) at 37 °C. From Fig. 3, the rates and amounts of DOX released from the NP/D nanocomposite strongly depended on the pH value and release time. NP/D showed a much faster DOX release at pH 5.0 and 6.5 than at pH 7.4. As can be seen from Fig. 3, the cumulative release of DOX from NP/D is less than 18% after 35 h in the pH 7.4, which indicate that NP/D keep a rather good stability in the physiological condition. By comparison, a noticeably increased release of DOX is observed at pH 6.5 up to 40% and at pH 5.0 up to 65%, which demonstrated that the release rate of DOX from NP/D in acidic tumor micro-environment is much faster than that at pH 7.4. The release of DOX from the NP/D in an acidic tumor micro-environment is likely due to the relief of electrostatic interaction characteristics between the DOX molecules and the ND-PEG nanoparticles. It can be inferred that the NP/D nanoparticle exhibits relative high stability at physiological condition, whereas when NP/D reach into tumor cells, a large amount of DOX is released to inhibit the proliferation of the cancer cells. This pH-dependent releasing behaviour of the drug delivery system is highly desirable for achieving the tumor-targeted programmable delivery.

3.3. In vitro cytotoxicity

The NP/D was further investigated to evaluate the potential therapeutic efficacy. Here, the in vitro cytotoxicity of NP/D against HepG2, HeLa and MCF-7 cells was investigated by MTT assay, where

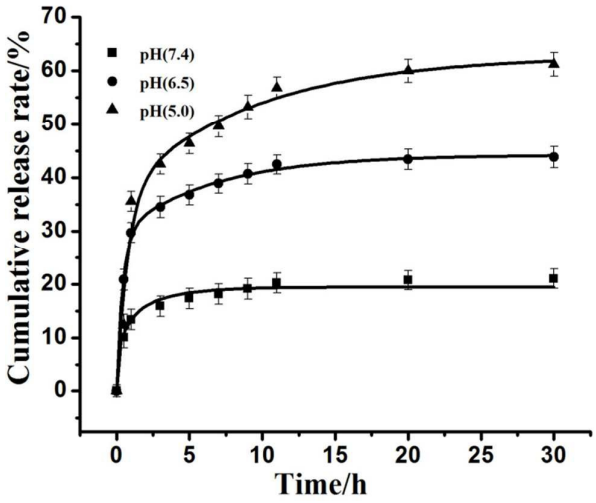

Fig. 3 Cumulative release of DOX from NP/D nanoparticles in different pH environments (PBS, p H 5.0 ( ), 6.5 ( ), 7.4 ( )) with time in vitro.

the cells were cultured in the suspensions of NP/D and free DOX solutions at a series of equivalent DOX dose for 72h, respectively. As shown in Fig. 4, The ND-PEG has no cytotoxic effect on cell viability, thus indicating that the carrier exhibit good biocompatibility, while both free DOX and NP/D were found to inhibit HepG2, HeLa and MCF-7 cells, and the relative cell viability declined monotonously with ascending the concentration of DOX. When the concentration of DOX was very low (1 $\mu g \cdot mL^{-1}$), both NP/D and free DOX had similar cytotoxicity effects on both HepG2 and HeLa cells, Nevertheless, NP/D obviously exhibit superior cytotoxicity on HepG2 cells than that of free DOX when the concentration increased. For example, the viability of HepG2 cells was 20 % for NP/D and 27 % for free DOX with 5 $\mu g \cdot mL^{-1}$ DOX. Furthermore, it was worthy note that NP/D with a low concentration exhibited a similar cytotoxicity to free DOX with a high concentration. For instance, the viability of the HepG2 cells was 24 % for free DOX with a concentration of 9 $\mu g \cdot mL^{-1}$, while it was 20 % for NP/D with just 5 $\mu g \cdot mL^{-1}$ of DOX, which indicated NP/D nanoparticles can significantly improve the drug efficacy of DOX.

In addition, the cytotoxicity of both NP/D and free DOX with incubation time was also investigated (Fig. S3). The result displayed that with the prolonged incubation time, the cancer cells viability treated with ND-PEG has not been significantly affected, which indicated that ND-PEG can be as a nanocarrier for cancer therapy. However, the cells viability treated with NP/D decreased as the incubation time goes on and gradually over the free DOX, which suggested that the slow and prolonged cellular uptake of the NP/D may delay the killing of the cancer cells.

3.4. In vitro scratch assay

As DOX significantly influenced the proliferation of cancer cells, we assumed whether the NP/D has the same effect on tumor cell migration, scratch assays were performed in the presence of 5 $\mu g \cdot mL^{-1}$ NP/D. As shown in Fig. 5A, the scratch width is evidently narrowed while MCF-7 cells treated by ND-PEG even if time

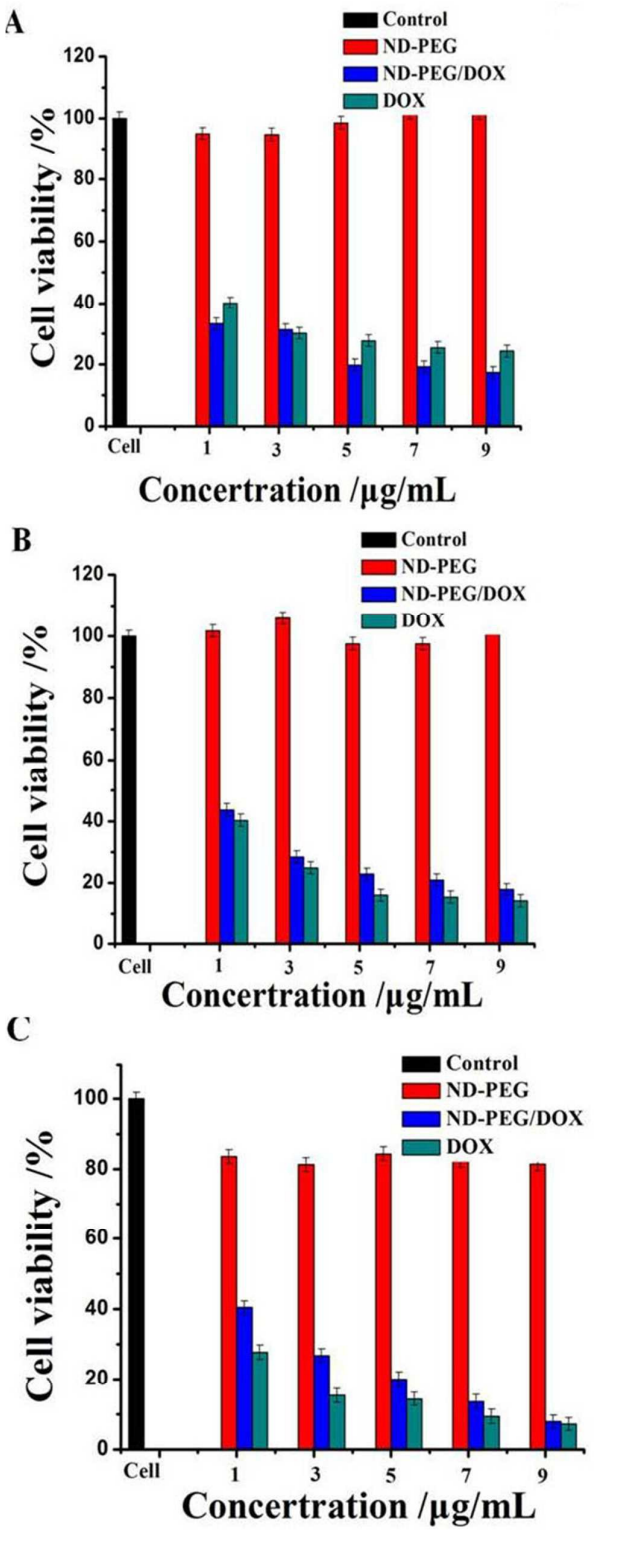

Fig. 4 Effect of ND-PEG, free DOX and NP/D on HepG2, HeLa and MCF-7 cells viability for 72 h was measured by MTT assay. (A) HepG2 cells, (B) HeLa cells and (C) MCF-7 cells. Experiments were repeated three times and data are presented as the mean ± SD (for each group, n = 6).

increases, which is similar to the control group, indicate that ND-PEG has almost no affect on the cell migration and can be applied as a nanocarrier for drug delivery, However the scratch width is nearly essentially unchanged while MCF-7 cells were treated with NP/D and DOX, the migration inhibiting rate of NP/D and DOX were up to 85 % and 86 % as shown in Fig. 5B, respectively, which verified our conjecture. Therefore, we learned that the NP/D can inhibit cell migration effectively.

3.5. Intracellular accumulation

Although the NP/D nanoparticles were found to be active, whether they have entered the cells or remained in the extracellular fluid was still unknown. Moreover, the therapeutic effect of DOX was dependent on its ability to inhibit the synthesis of nucleic acid through intercalation after entrance into nucleus. Therefore, to study whether the nanoparticles can enter living cells and DOX

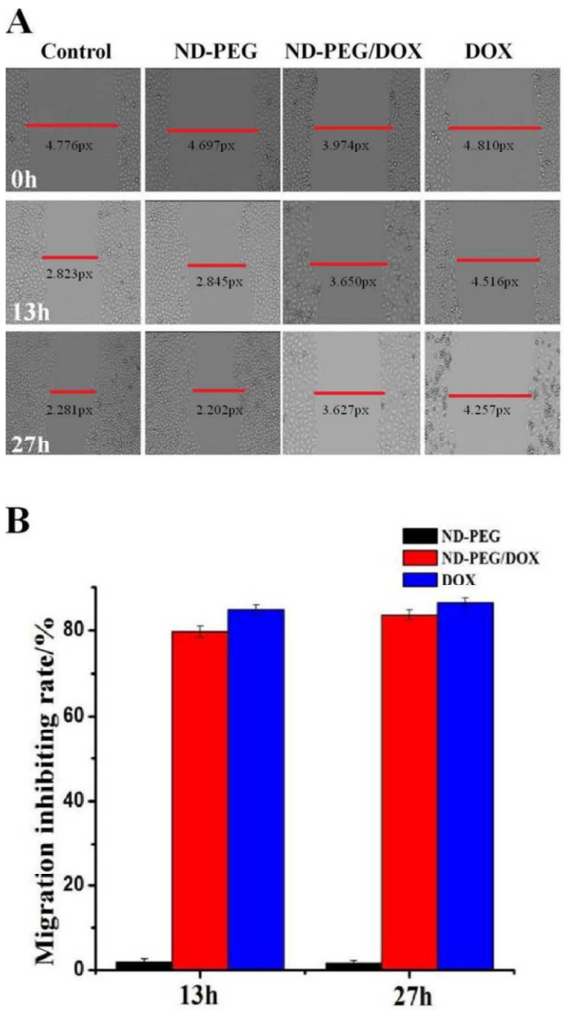

Fig. 5 The scratch assay of ND-PEG, NP/D and free DOX with time. (A) Representative images of MCF-7 cells treatment by ND-PEG, NP/D and free DOX, MCF-7 cells untreated as controls. (B) The migration inhibiting rate, where date were adopted from Fig. 5A.

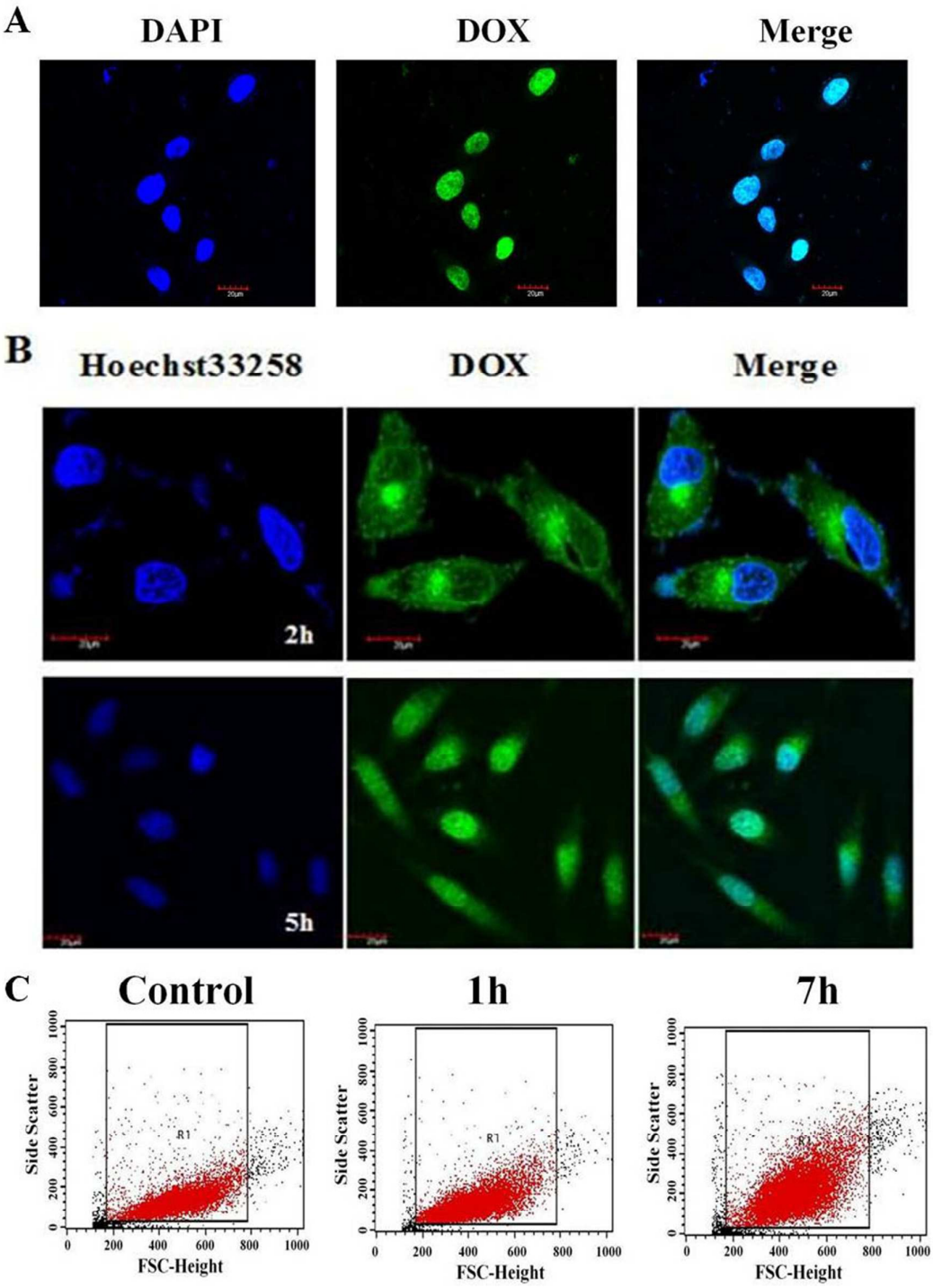

Fig. 6 Cellular uptake and distribution of NP/D nanoparticles. (A)Confocal laser scanning microscopy (CLSM) images of MCF-7 cells treated with free DOX for 1h. (B) Confocal laser scanning microscopy (CLSM) images of MCF-7 cells treated with NP/D in 2h and 5h, respectively. The images (A-B) in the left column show the cell nucleus dyed with DAPI for free DOX and Hoechst33258 for NP/D; the middle column shows DOX fluorescence, and the right column shows the merge of the two previous images. (C) The variations of side scatter (SS) after MCF-7 cells were treated with NP/D for 1h and 7h was quantified from a minimum of 10000 cells by Cell Quest software using flow cytometry analysis, respectively. Y-axis is side scatter (SS), which indicated intracellular particle complexity; X-axis is forward scatter (FSC)

dissociated from NP/D nanoparticles, we used laser scanning confocal microscopy with excitation wavelength of 488 nm and emission wavelength at 560-590 nm. As shown in Fig. 6A, free DOX efficiently entered into the cells and located in the cell nucleus after treatment for 1h which due to that free DOX accumulates in the nucleus by the simple passive diffusion between the extracellular and intracellular surroundings. In Fig. 6B, the weak green fluorescence intensity is mainly located in the cytoplasm but no signal in the nucleus after incubating 2h. When the incubation time was extended to 5h, the higher green fluorescence intensity is located in the nucleus of MCF-7 cells. Such a result implied that NP/D moved inside the cells and were capable of ferrying the drug inside living cells efficiently. Then DOX molecules were detached from the NP/D and followed migrating into the nucleus. This would lead to a sustained functional drug release compared to free DOX, which is consistent with the gradual DOX release from NP/D complexes in PBS at 37 °C (Fig. 3). The result was also accordant with the previous report by us, [26, 34-36] which indicated the potential applications of NP/D for controlled drug delivery.

Due to the fact that side scatter (SS) by flow cytometry analysis can indicate the particle complexities within the cells, the cellular uptake of NP/D can be indirectly demonstrated by SS. Fig. 6C showed that the SS of NP/D uptake by MCF-7 cells after 1h and 7h incubation, respectively. After coculture with NP/D for 1h, the value of SS only slightly increased, but it greatly increased after incubation 7h. The result suggests that the NP/D nanoparticles indeed enter the cells and the cell uptake is a time-dependent process.

To further examine the uptake kinetics of NP/D in cancer cells, MCF-7 cells were treated with 5 $\mu g \cdot mL^{-1}$ NP/D for different time and analyzed by flow cytometer. As shown in Fig. S4, the cellular uptake of NP/D and free DOX were greatly strengthened with time increased and the fluorescence intensity reached a plateau at about 7h for NP/D and 3h for free DOX. Curve fitting by single exponent function showed that the rate constants (k) of the endocytosis for NP/D was about 0.232 h^{-1}, namely, the value of uptake half-life was near 2.99 h, while the value of uptake half-life of free DOX was about 0.93 h, which indicated that the uptake rate of NP/D was approximately three times slower than free DOX. These results are related to cellular uptake pathways, where the uptake of DOX occurs through an energy-independent passive diffusion mechanism,[26] while the NP/D nanoparticles can efficiently delivery the drug inside living cells via clathrin-dependent endocytosis pathway (Fig. S5).

3.6. Cell apoptosis and cell cycle assay

As the above results revealed, NP/D has an efficient antitumor activity, then we further investigated the cell apoptosis behaviour of NP/D. From the qualitative analysis (Fig. S6), after treating cancer cells with 5 $\mu g \cdot mL^{-1}$ of NP/D for 48h and 72h, the cell morphology was examined under microscopy. In the control group, the cells were flat and adhered to the culture dish with high cell density. However, the cells treated with NP/D became long and slender. In addition, the cells turned into fragments and the cell density decreased. Thus, NP/D inhibited cancer cell proliferation and may have induced cancer cell apoptosis.

Soon afterwards, MCF-7 cells treated with 5 $\mu g \cdot mL^{-1}$ of NP/D were further double-stained with Annexin V/PI for flow cytometry to quantitative analysis of cell apoptosis (Fig. 7A). In the apoptosis quadrant diagram, each quadrant represents the living cells, early apoptosis cells, late apoptosis cells and debris cells in a counter clockwise direction from the bottom left**.** The results showed that about 33 % (the sum of late and early apoptosis) of cells were apoptotic after NP/D treatment and approximately 38 % of cells was apoptotic after free DOX treatment. The results again confirmed that DOX could efficiently release from NP/D in cells and resulted in cell apoptosis, and that mainly induced late cells apoptosis.

From the above results, it can be seen that the NP/D apparently induced cell apoptosis and inhibited cell migration. We made a hypothesis that the effect of NP/D knockdown on cell proliferation was regulated by the influence of cell cycle. We assessed the cell cycle phases in MCF-7 cells by flow cytometry. As shown in Fig. 7B, the number of cell distribution after NP/D knockdown was significantly increased in G2/M phase and concomitantly the number of cell distribution in G0/G1 phase was significantly decreased, while the number of cell distribution after free DOX knockdown was also significantly increased in G2/M phase and concomitantly the number of cell distribution in S phase was significantly decreased (Fig. 7B). Therefore, out data indicated that both the inhibition of knockdown NP/D and free DOX on cell proliferation was achieved by arresting the cells in the G2/M phase. In conclusion, the results indicated that NP/D could inhibit the growth and migration of MCF-7 cells and the mechanism was regulation of cell cycle to arrest the cells in G2/M phase.

4. Conclusions

In this work, a novel technique was presented for preparing ND-PEG/DOX nanoparticle and achieving almost sixteen fold improvement in DOX loadings in comparison to previously reported techniques. The NP/D system exhibited excellent physiological stability and pH controlled drug release with high cytotoxicity compared to free drug. What is more, flow cytometer and confocal microscope analysis proved that NP/D can easily pass into cells and constantly sustained releasing DOX to nucleus, which indicated that the NP/D system has a slow and sustained drug release capability. It was also illustrated that NP/D could markedly inhibit the migration of cells. Finally, we obtained that NP/D could induce cell apoptosis, which is mainly late apoptosis-dependence, and NP/D could change the cell cycle compare to free drug. These studies will provide guidelines for developing smart nanoparticles for drug delivery applications.

Acknowledgement

This work is supported by the National Natural Science Foundation of China (Grant No. 21071091), Shanxi Science and Technology Development Program (Grant No. 20130313021-1).

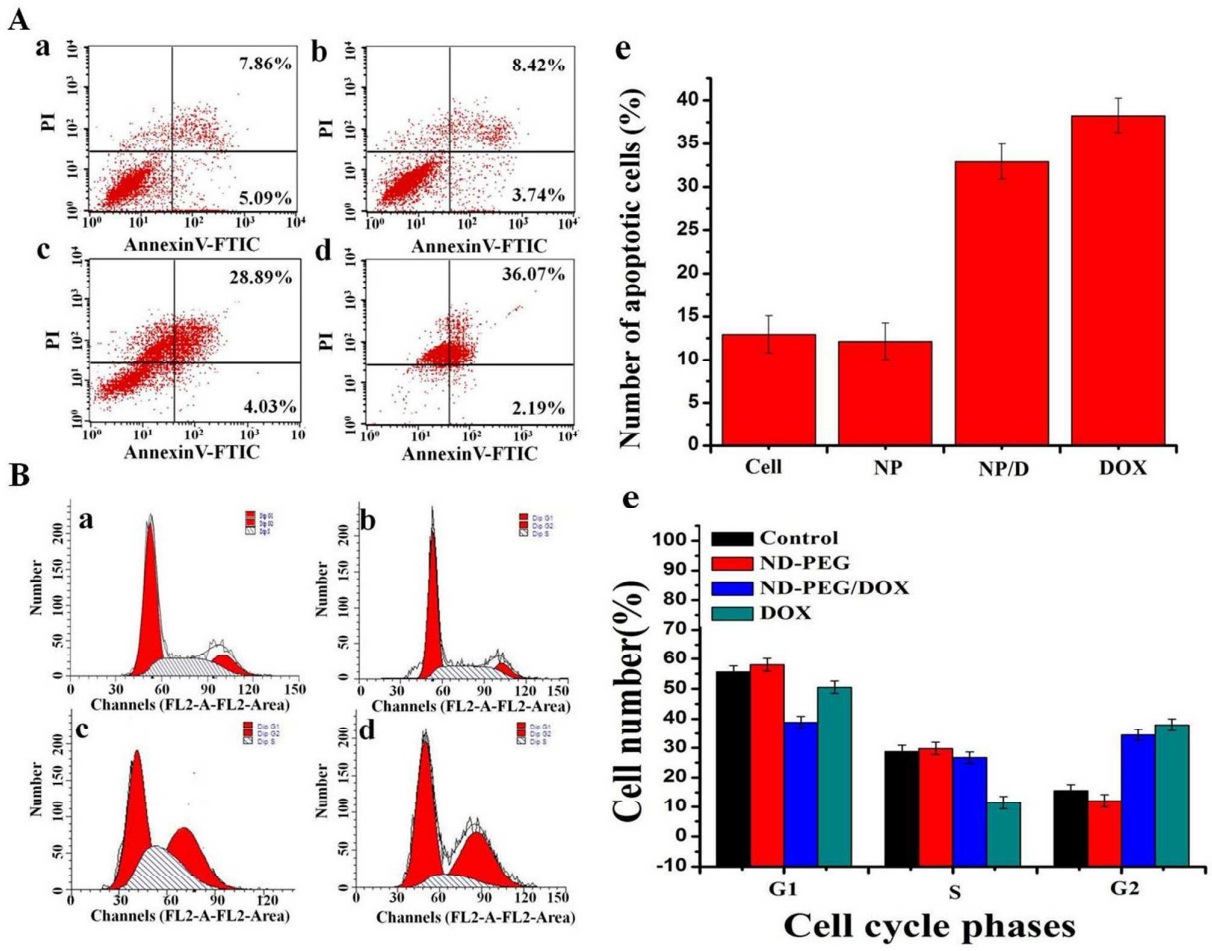

Fig. 7 Flow cytometry analysis. (A) Apoptosis of MCF-7 cells induced by ND-PEG (b), NP/D (c) and DOX (d) for 48h, MCF-7 cells untreated as control (a), the number of apoptotic cells (e), where date were adopted from a,b,c and d. (B) Cell cycle of MCF-7 cells induced by ND-PEG (b), NP/D (c) and DOX (d), MCF-7 cells untreated as control (a), the cell cycle histogram (e), where date were adopted from a,b,c and d.

References

1 L. Brannon-Peppas and J. O. Blanchette, *Adv. Drug. Delivery. Rev.,* 2012, **64**, 206-212.
2 L. Zhou, Z. Li, Z. Liu, J. Ren and X. Qu, *Langmuir.,* 2013, **29**, 6396-6403
3 L. Brannon-Peppas and J. O. Blanchette, *Adv. Drug. Delivery. Rev.,* 2012, **64**, 206-212.
4 D. F. Qiu, S. Wang, Y. Q. Zheng and Z. X. Deng, *Nanotechnology.,* 2013, **24**, 1-8
5 V. R. N, S. R. Mane, A. Kishore, J. D. Sarma and R. Shunmugam, *Biomacromolecules.,* 2012, **13**, 221-230.
6 S. Shimomura, H. Matsuno and K. Tanaka, *Langmuir.,* 2013, **29**, 11087-11092.
7 T. Frohlich, D. Edinger, V. Russ and E. Wagner, *Eur. J. Pharm. Sci.,* 2012, **47**, 914-920.
8 M. A. Zoroddu, S. Medici, A. Ledda, V. M. Nurchi, J. I. Lachowicz and M. Peana, *Curr. Med. Chem.,* 2014, **21**, 3837-3853.
9 S. Suppia, K. Kasematsa, A. Ivaska, K. Kunnis-Beresa, M. Sihtmaea, I. Kurveta, V. Aruojaa and A. Kahru, *J. Hazard. Mater.,* 2015, **286**, 25-74.
10 H. Kim, H. B. Man, B. Saha, A. M. Kopaca, O. S. Lee, G. C. Schatz, D. Ho and W. K. Liu, *J. Phys. Chem. Lett.,* 2012, **3**, 3791-3797.
11 V. Vaijayanthimala, D. K. Lee, S. V. Kim, A. Yen, N. Tsai, D. Ho, H. C. Chang and O. Shenderova, *Expert. Opin. Drug. Deliv.,* 2015, **12**, 735-749.
12 P. C. Tsai, O. Y Chen, Y. K. Tzeng, Y. Y Hui, J. Y Guo, C. C. Wu, M. S. Chang and H. C Chang, *EPJ. Quantum. Technology.,* 2015, **2**, 1-12.
13 H. M. Chaudhary, A. S. Duttagupta, K. R. Jadhay, S. V. Chilajwar and V. J. Kadam, *Curr. Med. Chem.,* 2015, **12**, 271-281.
14 B. Guan, F. Zou and J. F. Zhi, *Small.,* 2010, **6**, 1514-1519.

15 J. Li, Y. Zhu, W. X. Li, X. Y. Zhang, Y. Peng and Q. Huang, *Biomaterials.,* 2010, **31**, 8410-8418.
16 A. Adnan, R. Lam, H. Chen, J. Lee, D. J. Schaffer, A. S. Barnard, G. C. Schatz, D. Ho and W. K. Liu, *Mol. Pharmaceutics.,* 2011, **8**, 368-374.
17 A. Hegyi and E. Yablonovitch, *J. Biomed. Opt.,* 2013, **19**, 011015.
18 X. Y. Zhang, J. L. Yin, C. Kang, J. Li, Y. Zhu, W. X. Li, Q. Huang and Z. Y. Zhu, *Toxicol. Lett.,* 2010, **198**, 237-243.
19 D. J. Lim, M. Sim, L. Oh, K. Lim and H. Park, *Arch. Pharm. Res.,* 2014, **37**, 43-52.
20 Q. W. Zhang, V. N. Mochalin, I. Neitzel, K. Hazelia, J. J. Niu, A. Kontsosa, J. G. Zhou, P. I. Lelkesc and Y. Gogotsi, *Biomaterials.,* 2012, **33**, 5067-5075.
21 J. C. Arnault, T. Petit, H. Girard, A. Chavanne, C. Gesset, M. Sennour and M. Chaigneau, *Phys. Chem. Chem. Phys.,* 2011, **13**, 11481-11487.
22 J. Tisler, R. Reuter, A. Lammle, F. Jelezko, G. Balasubramanian, P. R. Hemmer, F. Reinhard and J. Wrachtrup, *ACS Nano.,* 2011, **5**, 7893-7898.
23 I. Neitzel, V. Mochalin, I. Knoke, G. R. Palmese and Y. Gogotsi, *Compos. Sci. Technol.,* 2011, **71**, 710-716.
24 T. K. Ryu, G. J. Lee, C. K. Rhee and S. W. Choi, *Macromol. Biosci.,* 2015, **15**, 1469-1475.
25 G. F. Xi, E. Robinson, B. Mania-Farnell, E. F. Vanin, K. W. Shim, T. Takao, E. V. Allender, C. S. Mayanil, M. B. Soares, D. Ho and T. Tomita, *Nanomedicine.,* 2014, **10**, 381-391.
26 Y. Q. Li, X. P. Zhou, D. X. Wang, B. S. Yang and P. Yang, *J. Mater. Chem.,* 2011, **21**, 16406-16412.
27 E. Osawa and D. Ho, *Springer: New York.,* 2010, **PP**, 1-33.
28 P. Villalbaa, M. K. Rama, H. Gomeza, V. Bhethanabotla, M. N. Helms and A. Kumar, *Mat. Sci. Eng. C.,* 2012, **32**, 594-598.
29 I. Cha, K. Hashimotob, T. Fujikic, T. Yamauchi and N. Tsubokawa, *Mater. Chem. Phys.,* 2014, **143**, 1131-1138.
30 M. F. Weng, S. Y. Chiang, N. S. Wang and H. Niu, *Diam. Relat. Mater.,* 2009, **18**, 587-591.
31 X. Y. Zhang, C. K. Fu, L. Feng, Y. Ji, L. Tao, Q. Huang, S. X. Li and Y. Wei, *Polymer.,* 2012, **53**, 3178-3184.
32 X. Y. Zhang, S. O. Wang, C. K. Fu, L. Feng, Y. Ji, L. Tao, S. X. Li and Y. Wei, *Polym. Chem.,* 2012, **3**, 2716-2719.
33 Y. Q. Li and X. P. Zhou, *Diam. Relat. Mater.,* 2010, **19**, 1163-1167.
34 Z. Q. Wang, Z. M. Tian, Y. Dong, L. Li, L. Tian, Y. Q. Li and B. S. Yang, *Diam. Relat. Mater.,* 2015, **58**, 84-93.
35 D. X. Wang, Y. L. Tong, Y. Q. Li, Z. M. Tian, R. X. Cao and B. S. Yang, *Diam. Relat. Mater.,* 2013, **36**, 26-34.
36 Y. Dong, R. X. Cao, Y. Q. Li, Z. Q. Wang, L. Li and L. Tian, *RSC Adv.,* 2015, **5**, 82711-82716.
37 A. D. Salaam, P. T. J. Hwang, A. Poonawalla, H. N. Green, H. W. Jun and D. Dean, *Nanotechnology.,* 2014, **25**, 425103.
38 A. V. Isabel, S. R. Laura, G. P. Laura, L. G. Antonio and D. Yolanda, *Exp. Eye. Res.,* 2014, **125**, 183-192.
39 F. Q. Hu, Y. Y. Zhang, J. You, H. Yuan and Y. Z. Du, *Mol. Pharmaceutics.*, 2012, **9**, 2469-2478.
40 D. X. Wang, Y. Q. Li and B. S. Yang, *Acta Chim. Sinica.,* 2013, **71**, 782-786.
41 E. K. Chow, X. Q. Zhang, M. Chen, R. Lam, E. Robinson, H. J. Huang, D. Schaffer, E. Osawa, A. Goga and D. Ho, *Sci Transl Med.,* 2011, **9**, 73ra21.
42 B. Liu, H. Y. Chen, X. Li, C. N. Zhao, Y. K. Liu, L. J. Zhu, H. P. Deng, J. C. Li, G. L. Li, F. L. Guo and X. Y. Zhu, *RSC Adv.,* 2014, **4**, 48943-48951.